Predicting permeability tensors of foams using vector kinetic method

Y Jobic, P Kumar, F Topin, R Occelli

Predicting permeability tensors of foams using vector kinetic method

Y Jobic[1], **P Kumar**[1], **F Topin**[1] **and R Occelli**[1]
[1]Laboratoire IUSTI, CNRS UMR 7343, Aix-Marseille Université
5, Rue Enrico Fermi, 13453 Marseille Cedex 13, France

E-mail: yann.jobic@univ-amu.fr

Abstract. Light cellular materials are increasingly used in many engineering applications due to several attractive properties including heat and mass transfer enhancement, low pressure drop compared to packed bed of spheres. It is therefore important to simulate the complex and unsteady flows by reliable numerical methods to determine intrinsic macroscopic hydraulic properties on actual foam structures. The approach of numerical simulations at pore scale has become popular criterion with the development of high performance computational power. Numerical studies based on a type of Lattice Boltzmann Method (LBM) were performed in the present work. Another kinetic method than LBM has been explored. A vector kinetic method is proposed which has the advantage of being non-diffusive, explicit, parallel, and use only physical variables instead of discrete velocity. The proposed numerical method is validated against experimental and numerical permeability data obtained on idealized isotropic idealized as well as real foam samples.

1. Introduction

Transport phenomena in different porous media have been studied for nearly two centuries. However, the works on high porosity porous media i.e. open-cell foams are still relatively few and recent. Analytical models used for conventional porous media such as packed bed of spheres are not directly applicable on foams [1]. A number of studies to characterize hydraulic properties of foams have been undertaken to fill this gap. On the other hand, experimental and numerical results characterizing the pressure drop in the foams are highly dispersed [2]. Because of advances in 3D imaging techniques, an emerging trend is the determination of intrinsic hydraulic parameters from flow laws on reconstructed geometries using 3-D direct numerical simulations, often using commercial tools [3]. In the present work, a new kinetic approach is presented to solve transport equations at local scale and determine the macroscopic permeability. This approach is also capable of determining morphological properties of different foam samples as well as complex/heterogeneous media.

2. Numerical method

The numerical method called "FVS-BGK" developed in the present work comes from a rigorous use of the kinetic theory [4]. It is based on a collisional operator of type BGK (simpler collisional operator of the Boltzmann equation) [5], and can be written as:

[1]Y Jobic: yann.jobic@univ-amu.fr.

$$\partial_t f + \frac{1}{\epsilon_{adv}} \mathbf{v}(\xi) \cdot \nabla_{\mathbf{x}} f = \frac{1}{\epsilon_{coll}} (M[W] - f) \tag{1}$$

We are considering a vectorial BGK, with one component per unknown (here density and velocity).The velocity space has been discretized, using a 2D points stencil, D being the dimension of the problem, and $\xi \in [0,2D]$, the considered discrete velocity. ϵ_{adv} and ϵ_{coll} are small positive parameters that will tend to zero in a special way. W are the moments of the maxwellian equilibrium M. This kinetic equation approximate the following system of conservation laws:

$$\partial_t W + \sum_{j=1}^{D} \frac{\partial}{\partial x_j} F_j(W) = 0 \tag{2}$$

Naming F_j the flux of W. For equation (2) to be consistent with equation (1), we must have:

$$\int M[W](\xi) d\xi = 0 \tag{3}$$

$$\int v_j(\xi) M[W](\xi) d\xi = F_j(W) \tag{4}$$

The challenging task is to define M so that the model conserves a kinetic convex entropy η, as well at the continuous level than at discrete level. The chosen form of M is linear with respect to W and F_j. The existence of the associated entropy η (and her flux) will leads to a sub-characteristics condition on the stability of the scheme. We will solve equation (1) by a transport-projection algorithm [6]. The projection step consists in replacing f in the right hand side (RHS) of equation (1) by $M[W]$ at each time step:

$$f(t_n, x, \xi) = M[W^n(x)](\xi) \tag{5}$$

By doing this, the RHS of equation (1) is zero. The projection step has some interesting features; the most important one is that all the kinetic variables will be eliminated in the final scheme, using only the dimensioned macroscopic physical variables (density, velocity). The transport/projection algorithm, discretized in space, will be interpreted as a Flux Vector Splitting (FVS) method. This will enables to import the continuous kinetic entropy condition to the discrete level.

We are now seeking the limit of equation (1) when ϵ_{coll} tends towards zero while setting $\epsilon_{adv} \approx \sqrt{\epsilon_{coll}}$ (see [7]), which leads to the simplified system:

$$\left.\begin{aligned} \partial_t \rho + \nabla_x \cdot (\rho u) = 0 \\ \partial_t (\rho u) + \nabla_x \cdot \left(\rho u \otimes u + \frac{P(\rho)}{\epsilon^2} I \right) = 0 \end{aligned}\right\} \tag{6}$$

Note that the associated Mach number is of the order of ϵ_{adv} leading to the so called low Mach number limit. By passing to the limit, and assuming a constant fictive temperature, we can write:

$$\rho \to \bar{\rho}, \frac{P(\rho) - P(\bar{\rho})}{\epsilon^2} \to \bar{\rho} p \tag{7}$$

Where, p is the physical pressure, $P(\rho)$ the pressure law and $\overline{\rho}$ the referenced density.

We choose $P(\rho) = c_s^2 \rho$. In this limit, we therefore obtain the incompressible Euler equations. In order to have the incompressible Navier-Stokes equation (INSE), we need to add the diffusive term. To do this, the idea is to fully define the numerical diffusion coming out from the discrete numerical scheme,

and to fix accordingly the free parameters of the current scheme to the desired physical diffusion leading to the following formula (consistency):

$$\epsilon = \frac{c\Delta x}{2\nu} \tag{8}$$

As the scheme is explicit in time, CFL can be described as:

$$2D\frac{\nu\Delta t}{\Delta x^2} \leq 1 \tag{9}$$

Finally, the numerical scheme in terms of density and dimensioned physical velocity is written as:

$$\left.\begin{aligned} \rho_i^{n+1} &= \left(1 - 2D\frac{\nu\Delta t}{\Delta x^2}\right)\rho_i^n + \frac{\nu\Delta t}{\Delta x^2}\sum_j^D \rho_{i-e_j}^n + \frac{\Delta x}{2\nu}(\rho u_j)_{i-e_j}^n + \rho_{i+e_j}^n - \frac{\Delta x}{2\nu}(\rho u_j)_{i+e_j}^n \\ (\rho u)_i^{n+1} &= \left(1 - 2D\frac{\nu\Delta t}{\Delta x^2}\right)(\rho u)_i^n \\ &+ \frac{\nu\Delta t}{\Delta x^2}\sum_j^D \left((\rho u)_{i-e_j}^n + \frac{\Delta x}{2\nu}(\rho u)_{i-e_j}^n + \frac{2\nu}{\Delta x}\frac{P(\rho_{i-e_j}^n)}{c^2}e_j \right. \\ &\left. + (\rho u)_{i+e_j}^n + \frac{\Delta x}{2\nu}(\rho u)_{i+e_j}^n + \frac{2\nu}{\Delta x}\frac{P(\rho_{i+e_j}^n)}{c^2}e_j \right) \end{aligned}\right\} \tag{10}$$

One notices a sum with lots of terms in each moment, over *j*: this corresponds to the projection step (f forces to be Maxwellian). Finally, the sub-characteristic stability condition is then:

$$\frac{c_s}{1 - \frac{\Delta x}{2\nu}\max\limits_{i,j=1\ldots D}|u_{ij}|} \leq c \tag{11}$$

The initialization of parameters is as follows: we fix $\epsilon = 1$ (this parameter having no influence in the final scheme), finding c with consistency formula, then we fix the ratio $c_s/c = 1$ (as numerical tests proved this choice to provide good accuracy) finding the last parameter c_s.

3. Macroscopic equations

1-D approach (in each direction) of the pressure drop is adopted in this work (see Figure 1). Though the inertial effects can be significant at low Reynolds number in open-cell foams, it is necessary to determine permeability in Darcy regime [1] and verify the flow regime based on explored velocity range to choose the flow law in a coherent way. The Stokes equation can be averaged (neglecting the Brinkman correction) for Darcy's law:

$$-\overline{\overline{K_D}}\nabla\langle P\rangle = \mu_f\langle V\rangle \tag{12}$$

where, $\nabla\langle P\rangle$ is the average pressure gradient, $\overline{\overline{K_D}}$ is the permeability tensor, μ_f is the fluid viscosity and $\langle V\rangle$ is the average fluid velocity over all the volume of the foam sample.

In order to determine permeability tensors, the following boundary conditions were used:

- Prescribed pressure drop between the two opposite faces while other faces were set as symmetry planes as shown in Figure 1.
- The above boundary conditions were repeated three times to perform the numerical simulations with flow along the three basic directions.

The components of the averaged pressure gradient vector and average velocity gradient vector in each direction lead to the determination of permeability tensors as described below:

$$\overline{\overline{K_D}} = \begin{bmatrix} {K_D}^{xx} \\ {K_D}^{xy} \\ {K_D}^{xz} \\ {K_D}^{yy} \\ {K_D}^{yz} \\ {K_D}^{zz} \end{bmatrix} = \mu_f \begin{bmatrix} \nabla P_x^1 & \nabla P_y^1 & \nabla P_z^1 & & & \\ & \nabla P_x^1 & & \nabla P_y^1 & \nabla P_z^1 & \\ & & \nabla P_x^1 & & \nabla P_y^1 & \nabla P_z^1 \\ \nabla P_x^2 & \nabla P_y^2 & \nabla P_z^2 & & & \\ & \nabla P_x^2 & & \nabla P_y^2 & \nabla P_z^2 & \\ & & \nabla P_x^2 & & \nabla P_y^2 & \nabla P_z^2 \\ \nabla P_y^3 & \nabla P_z^3 & & \nabla P_y^3 & \nabla P_z^3 & \\ & \nabla P_y^3 & \nabla P_z^3 & & \nabla P_y^3 & \nabla P_z^3 \end{bmatrix}^{-1} \cdot \begin{bmatrix} {V_x}^1 \\ {V_y}^1 \\ {V_z}^1 \\ {V_x}^2 \\ {V_y}^2 \\ {V_z}^2 \\ {V_x}^3 \\ {V_y}^3 \\ {V_z}^3 \end{bmatrix} \quad (13)$$

In equation 13, subscripts x, y, z describe the directions while superscripts 1,2,3 describe the numerical simulation performed each time in a given direction. In case of isotropic foams, diagonal components of permeability tensors are equal while the other components are zero.

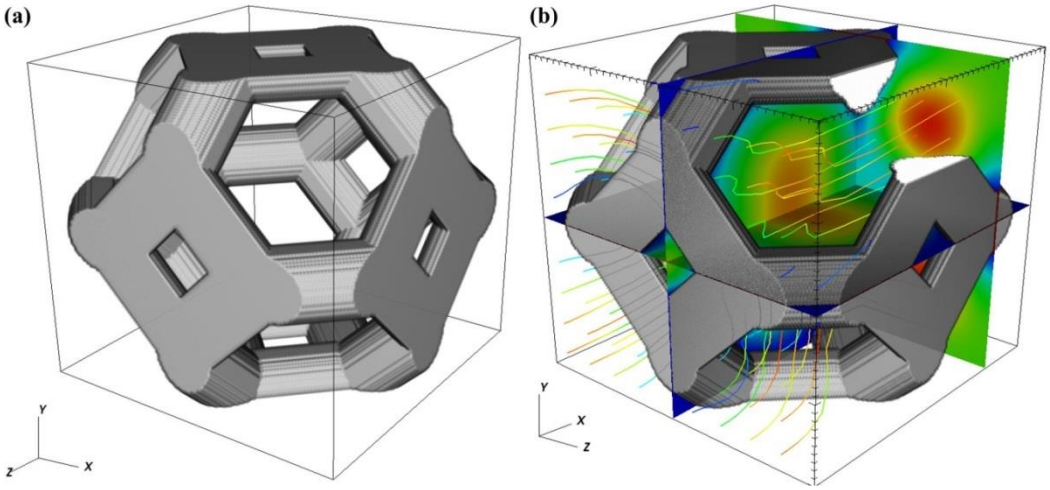

Figure 1. (a) Kelvin-like cell of d_{cell} =4mm (Resolution 160^3 points) (b) Flow field: velocity magnitude through the foam on two perpendicular planes.

The mean pressure gradient ($\nabla\langle P\rangle$) is the sum of two terms: the average of local pressure gradients and the sum of pressure forces on the solid-fluid interfaces. The mean pressure gradient can be determined in two ways. First method is by volume averaging of pressure gradients across the sample and measuring the resulting pressure forces at solid surface. The second method is by using the average pressure difference between the inlet and outlet faces of the medium [8]. The use of macroscopic fluid pressure requires a correction due to the surface porosity on these faces. $\nabla\langle P\rangle$ thus can be described as (see [1] for detailed description):

$$\nabla\langle P\rangle = \frac{\underbrace{\langle \nabla P \rangle}}{local\ pressure\ gradients} - \frac{\underbrace{\int P n_{sf} dA}}{forces\ on\ the\ solid-fluid\ interfaces} = \varepsilon_{sur} \frac{\Delta P}{L} \quad (14)$$

where, $\Delta P/L$ and ε_{sur} are pressure drop applied and surface porosity at the inlet and outlet faces.

Several numerically controlled and real foam samples of very different typologies were analysed. At first, a representative periodic cell (Kelvin-like cell) consisting of cylindrical struts was chosen for which it is easy to change the foam geometry (cell size, strut diameter, porosity and orthotropic anisotropy). Further, a commercial foam sample obtained from μCT tomography images (RECEMAT NC 1723) was tested [3].

The dimension of representative volume element (>5 cells) to perform numerical simulations was chosen in order to optimize results' reliability and computational time (see [3]). The calculations were performed until the values of Darcian permeability, K_D differed less than 1% between two consecutive mesh sizes. The simulations were stopped when variations of K_D were less than 0.1%. Moreover, we also systematically checked mass in-balance and that there were no variations in the global flow.

4. Global hydraulic results

4.1. Periodic-idealized Kelvin-like cell

4.1.1 Influence of mesh resolution

The mesh convergence is important to obtain results the closest possible to real cases and must be carefully done to not obtain a contrary effect. In fact, if the mesh is too thin, the solver reaches the point where there is no residual convergence and thus, no correct results can be obtained. On the other hand, coarse meshing does not allow the solver to provide accurate results as morphological errors are very important. The first step was to verify the impact of the geometric discretized resolution (voxel size) on porosity (ε_o), surface porosity (ε_{sur}), specific surface area (a_c) and permeability (K_D) values of the Kelvin-like foam sample of cylindrical strut shape (ε_o =0.80, see Kumar and Topin [1]) as presented in Figure 1 (see Table 1 and Figure 2).

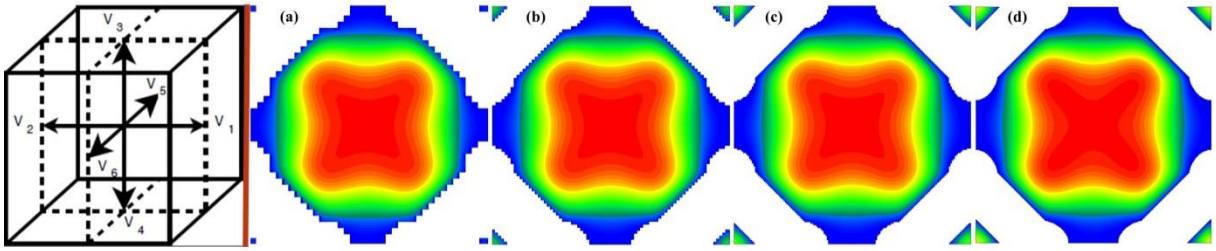

Figure 2. Left: 3-D discretization; Right: Velocity field in the middle plane (a) Resolution 40^3 points, (b) Resolution 80^3 points, (c) Resolution 160^3 points, (d) Resolution 320^3 points,

It can be observed that the morphological parameters start to converge at lower resolution to capture precisely the 3-D foam structure reported in the works of Kumar and Topin [1]. On the other hand, the main flow topology is well captured despite the loss of resolution. The calculated permeability converges when resolution decreases and is comparable to that reported in [1]. To perform parametric studies, 160^3 mesh cells were chosen to perform optimised numerical simulations without compromising accuracy of the data (see Table 1 and Figure 2).

Table 1. Mesh influence on morphology and permeability to quantify geometric discretization error.

Resolution		Morphological properties			Permeability, K_D (m^2)
Voxel size (m)	Number of mesh cells	Porosity (ε_o)	Surface Porosity (ε_{sur})	Specific surface area, a_c (m^{-1})	
0.00011	40^3	0.7656	0.5789	869.30	1.3764E-07
5.13e-05	80^3	0.774	0.6358	874.78	1.2729E-07
2.53e-05	**160^3**	**0.7863**	**0.6735**	**867.17**	**1.2710E-07**
1.26e-05	320^3	0.7921	0.691	864.58	1.2722E-07

4.1.2 Verification of homothetic scaling-law

Several virtual homothetic foams of different cell diameters/sizes (d_{cell}) for a given porosity (ε_o) as well as foam samples of different porosities by changing the strut size for a given cell size (similar to the works of Kumar and Topin [1]) have been generated as presented in Table 2 (considering circular strut shape). By generating this set of virtual samples, we could assess individually the impact of pore size and porosity on permeability and thus evaluate the reliability of usage of classic description such as Ergun-like approach [9] for such materials. As expected, the permeability varies proportionally to the square of the cell size i.e. $K_D \propto {d_{cell}}^2$ (Figure 3a). Note that for real samples, porosity and pore shape usually vary with size which makes it difficult to compare directly with experimental data.

Table 2. Morphological parameters and permeability values of virtual foam samples.

Type of foams	Porosity, ε_o $(-)$	Cell size, d_{cell} (mm)	Surface Porosity, ε_{sur} $(-)$	Permeability, K_D (m^2)
Homothetic foam samples	0.7864	4	0.6734	1.27E-07
		3	0.6734	7.14E-08
		2	0.6734	3.18E-08
		1	0.6734	7.94E-09
		0.5	0.6734	1.99E-09
		0.25	0.6734	4.97E-10
Foam samples based on constant cell diameter	0.6306	4	0.5373	6.80E-08
	0.6828	4	0.5831	8.40E-08
	0.7358	4	0.6279	1.04E-07
	0.7864	4	0.6734	1.27E-07
	0.8373	4	0.7282	1.56E-07
	0.8897	4	0.7754	2.00E-07
	0.9429	4	0.8446	2.70E-07

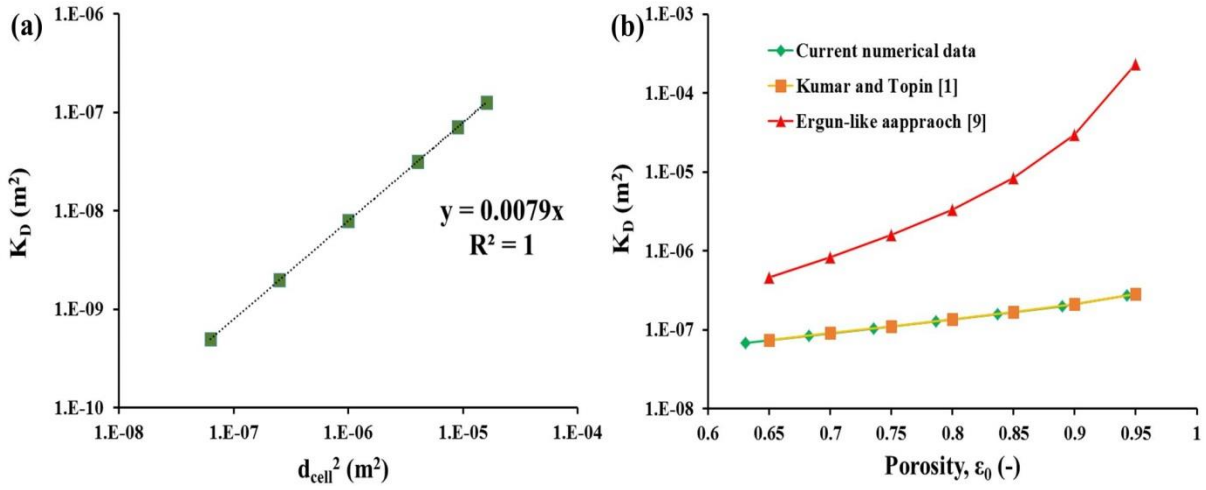

Figure 3. (a) Darcian permeability as a function of square of cell diameter/size for a constant porosity. (b) Validation and comparison of Darcian permeability as a function of porosity for a given cell size (d_{cell} =4mm).

4.1.3 Influence of porosity at constant cell diameter

The current numerical results obtained from VFS-BGK on structured grid were compared against analytical approach of Ergun [9] ($K_D = 150\,{a_c}^2.(1-\varepsilon_o)^2/{\varepsilon_o}^3$) and numerical results of Kumar and Topin [1] obtained on commercial software (StarCCM+) on polyhedral meshing. The classical analytical description of permeability with the morphological parameters of the foam structure is

based on Ergun-like approach that was originally developed for packed bed of spheres. Most commonly, permeability was linked to two parameters i.e. pore size and porosity for isotropic and commercially available foams.

From the Figure 3b, it is observed that the current numerical data and data from the works of Kumar and Topin [1] coincide perfectly. On the other hand, the offset points corresponding to proposed work come from the different discretization (including some morphological error) as a function of resolution. The proposed discretization method causes errors at the walls according to the resolution where thin or sharp edges of strut shape of foam structure under voxel resolution are not visible. It can also be seen that the Ergun-like formulation does not clearly follow the same trend as obtained numerically to describe permeability in the whole porosity range and thus, cannot be reliably applied to open-cell foams.

4.2 Real foam samples of high porosity

A commercial foam sample has been chosen on which experimental and numerical studies of pressure drop have already been performed (an image of NC 1723 foam in Figure 4a). The geometry has been reconstructed from the μCT tomographic images using 198x198x342 voxels. The domain (representative elementary volume) used for flow simulations is identical to that reported in the work of Brun et al., [3]. An excellent is obtained between experimental and numerical results with current results (see Figure 4b). Note that the permeability reported experimentally or numerically was Forchheimer permeability (see Kumar and Topin [1]). On the other hand, the permeability obtained using proposed method is actually Darcian permeability (K_D) and of value $3.57 \times 10^{-8}\, m^2$. Moreover, it is difficult to assess accurately the bias between Darcian and Forchheimer permeability.

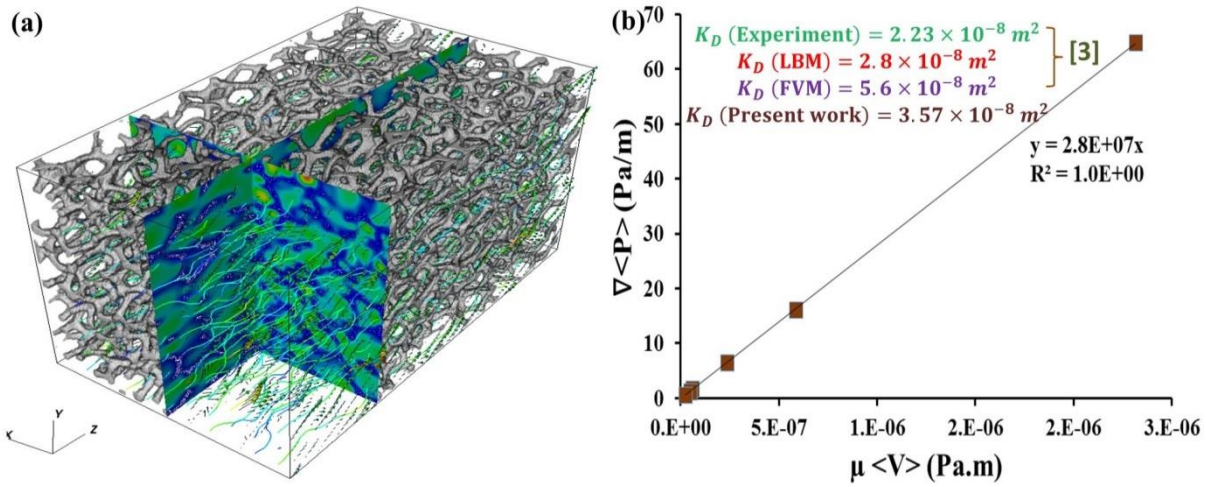

Figure 4. (a) 3-D reconstruction and flow field of NC1723 foam sample (ε_o =0.87); (b) Comparison and validation of permeability with literature data and current numerical data.

4.3 Application to anisotropic media (orthotropic case)

Based on the comparison and validations performed on idealized and real open cell foams of different porosities, the proposed method gives reliable permeability values. It can thus, be very interesting to obtain permeability tensors on orthotropic foams as available literature data are very scarce (see Hugo [10]). Orthotropic anisotropy of the original foam sample was realized by elongating and compressing simultaneously in two orthogonal directions by a factor $\sqrt{\Omega}$ and $1/\sqrt{\Omega}$ while the third direction is kept unaffected to conserve porosity of the original sample. An anisotropic foam sample of Kelvin-like cell constituting circular strut shape is presented in Figure 5a.

For fluid flow simulations, the sections in the X, Y and Z-directions of the unit periodic cell are presented in Figure 5b. The calculations were repeated successively in the three directions to determine permeability tensors (see Equation 13 in section 3). The permeability tensors are presented in Table 3. It can be observed that permeability first increases and then decreases in the elongation direction (i.e. in X-direction). On the other hand, permeability deceases in other two directions (i.e. Y and Z-directions). No physical interpretation has been yet found to describe the permeability nature in orthotropic foams.

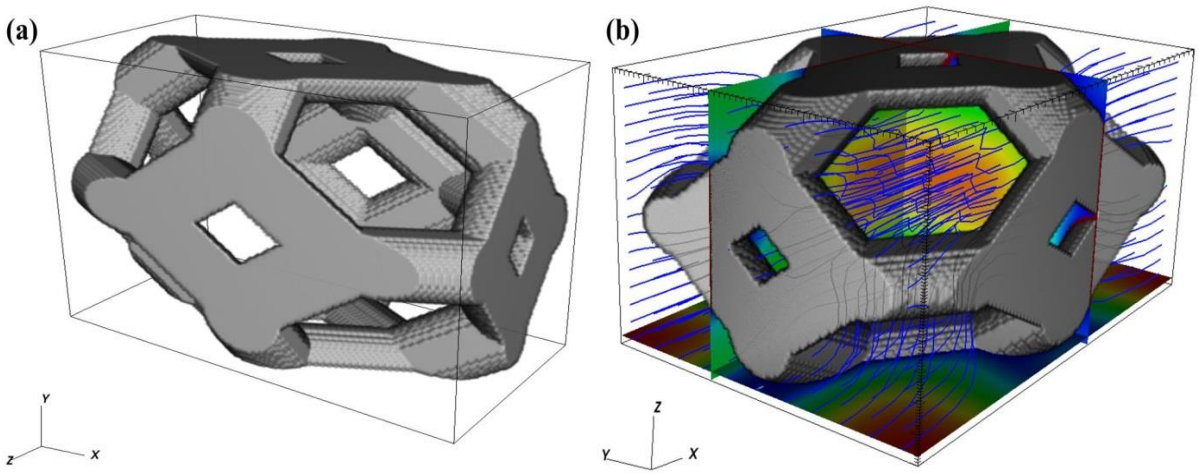

Figure 5. (a) An image of orthotropic foam; (b) Velocity field through orthotropic foam.

Table 3. Permeability tensors in X, Y and Z-directions of a virtual orthotropic foam sample.

ε_o (-) [1]	Ω (-)	ε_o (-)	${K_D}^{xx}$ (m^2)	${K_D}^{yy}$ (m^2)	${K_D}^{zz}$ (m^2)
0.80	1	0.786	1.27E-07	1.27E-07	1.27E-07
	2	0.781	1.7E-07	1.2E-07	7.6E-08
	3	0.778	1.65E-07	1.07E-07	5.72E-08
	4	0.779	1.5E-07	9.55E-08	4.87E-08

5. Conclusion

Lattice Boltzmann Method has been used extensively to characterize the effective properties of foams. To overcome its limitations, another kinetic tool "VFS-BGK" has been developed in the present work. Current numerical results showed that the new method characterizes precisely the Darcian permeability tensors, demonstrating its accuracy and robustness. Present data have been compared and validated against experimental and numerical data reported in the literature and are in complete coherence; exhibiting that the numerical tool is well suited for permeability tensors determination.

References

[1] Kumar P and Topin F, Transp. Porous Media. 105-1 (2014), 57-81.
[2] Bonnet J-P, Topin F and Tadrist L, Transp.Porous Med. 73 (2008), 233-254.
[3] Brun E, Vicente J, Topin F, Occelli R and Clifton M J, Adv. Eng. Mat. 11-10 (2009), 805-810.
[4] Carfora M and Natalini R, ESAIM: Math. Modelling Numer. Anal. 42 (2008), 93-112.
[5] Krook M, Bhatnagar P L, and Gross E P, Phys. Rev. 94 (1954), 511.
[6] Bouchut F, Numer. Math. 94 (2003), 623-672.
[7] Bouchut F, Guarguaglini F R and Natalini R, Indiana Univ. Math. J. 49 (2000), 723-749.
[8] Renard P, Genty A and Stauffer F, J. Geophysical Res. 106-B11 (2001), 26443-26452.
[9] Ergun S, Chem. Eng. Prog. 48 (1952), 89–94.
[10] Hugo J-M, PhD thesis, Aix-Marseille Université.